Estimating Space Environment Effects during All-Electric Telecom Satellite Missions

IEPC-2017-474

Presented at the 35th International Electric Propulsion Conference
Georgia Institute of Technology • Atlanta, Georgia • USA
October 8 – 12, 2017

J.-C. Matéo-Vélez[1], L. Artola[2], N. Bérend[3], J.-P. David[4], B. Dirassen[5], G. Hubert[6], C. Inguimbert[7], D. Lazaro[8], Th. Nuns[9], D. Packan[10], Th. Paulmier[11] and P. Sarrailh[12]

ONERA, The French Aerospace lab, 2 avenue Edouard Belin, 31055-Toulouse, France

Abstract: The benefits of using electric propulsion for geostationary orbit spacecraft, including station keeping and orbit raising, consists for operators in the reduction of mission costs through higher dry mass to orbit in comparison to classical chemical propulsion. The disadvantages of this strategy rely on the significantly increased amount of time spent within the radiation belts during orbit raising. The radiation dose involves long-term degradation as well as sporadic effects on external and internal equipment. In this paper, an analysis of the radiation effects is performed assuming several scenarios for an electrical orbit raising to geostationary orbit. Environments specifications are used to estimate the effect of high energy particles on optoelectronic and integrated electronic components, on solar cell performance and on the occurrence of internal and external electrostatic discharges.

Nomenclature

D	=	Charge carrier diffusion coefficient
I_{sp}	=	Specific impulse
T/W	=	Thrust to weight ratio
τ	=	Charge carrier lifetime
V_{th}	=	Thermal velocity

[1] Research engineer at the Physics, Instrumentation, Environment and Space Department, Mateo@onera.fr
[2] Research engineer at the Physics, Instrumentation, Environment and Space Department, Laurent.Artola@onera.fr
[3] Research engineer at the Information Processing and Systems Department, Nicolas.Berend@onera.fr
[4] Research engineer at the Physics, Instrumentation, Environment and Space Department, Jean-Pierre.David@onera.fr
[5] Research engineer at the Physics, Instrumentation, Environment and Space Department, Bernard.Dirassen@onera.fr
[6] Research engineer at the Physics, Instrumentation, Environment and Space Department, Guillaume.Hubert@onera.fr
[7] Research engineer at the Physics, Instrumentation, Environment and Space Department, Christophe.Inguimbert@onera.fr
[8] Research engineer at the Physics, Instrumentation, Environment and Space Department, Didier.Lazaro@onera.fr
[9] Research engineer at the Physics, Instrumentation, Environment and Space Department, Thierry.Nuns@onera.fr
[10] Research engineer at the Physics, Instrumentation, Environment and Space Department, Denis.Packan@onera.fr
[11] Research engineer at the Physics, Instrumentation, Environment and Space Department, Thierry.Paulmier@onera.fr
[12] Research engineer at the Physics, Instrumentation, Environment and Space Department, Pierre.Sarrailh@onera.fr

I. Introduction

More and more spacecraft use electric propulsion to reach geostationary Earth orbit (GEO). All electric architecture allows increasing the payload or choosing costless launches because the propellant mass is significantly reduced with respect to chemical propulsion. The side effect of it, however, is to spend a larger amount of time in the geostationary transfer orbit (GTO), resulting in more significant radiation constraints. The electric orbit raising (EOR) spacecraft launched in 2015 (Eutelsat 175 West B and ABS 3A) spent 5 to 7 months in GTO and, more recently, the Eutelsat 172 B and Viasat-2 spacecraft launched in June 2017 also spent a few months to reach GEO, instead of a few days for classical propulsion. The prolonged exposure to radiation can be estimated by analyzing flight data and/or performing ground experiments and running numerical simulations. The external environment of spacecraft orbiting the Earth is composed of energetic particles trapped within the radiation belts. It was shown in Ref 1. that a 220 day GTO transfer by electric propulsion adds an ionizing dose of around 25 krad to the nominal 50 krad dose received during a 15 years GEO mission, considering AX8 models for trapped particles[2,3]. In addition, the self-produced environment is composed of low energy charged and neutral particles emitted by the electrical thrusters. Both types of particles impact the behavior and longevity of materials and components on-board.

Space and self-produced environments effects are covered by the multiple physics numerical tools developed by ONERA from decades of research activities in the field of modelling the space environment and its effects. The effects depend on the environmental inputs to be provided by mission analysis. Trajectories may come from actual spacecraft data provided by NORAD (https://www.celestrak.com/NORAD/elements/) or by orbit generation tools such as embedded in OMERE (http://www.trad.fr/OMERE-Software.html). ONERA also developed a tool to compute simplified EOR trajectories. The environment along the orbit must be specified using well-recognized models such as AX8[2,3] or IGE_2006 at GEO[4], and standards such as ECSS and NASA guidelines[5,6]. Computed dose levels and particle fluence are then used as inputs for a series of numerical codes computing the effects on spacecraft components. These models are continuously upgraded and validated experimentally. The GDF-TK application based on Geant4 (http://space-env.esa.int/index.php/geant4-radiation-analysis-for-space.html) computes the transport of particles through spacecraft shielding and at component level. MUSCA-SEP 3 performs operational single event effects (SEE) risk assessment[7]. It is dedicated to hardening activities and anticipates trends for future technologies and reduce the occurrence and the effects of single event upset (SEU) for instance. MC-Solar models the degradation of solar cell performance due to damage dose[8]. SPIS-IC computes the transport of particles trapped inside internal dielectrics and allows estimating electric potential differences in complex 3D shapes such as printed circuit board or pin connectors[9], offering detailed information on electrostatic discharge risks. The SPIS software, initiated by ESA and CNES in the 2000's and developed mainly by ONERA and ARTENUM, assesses spacecraft surface charging under low energy plasma worst-cases of ECSS and NASA guidelines (www.spis.org). A second part of the effects taken into account in our tools covers particles generated by the spacecraft itself. Outgassing and contamination is handled by the COMOVA software on complex 3D geometries[10,11] and the plume side effects of the electric propulsion are introduced in SPIS[12,13].

This paper aims at estimating the radiation dose levels during the transfer to geosynchronous orbit by low-thrust electric propulsion and at measuring or predicting its effects on a series of sensitive equipment. It combines experimental campaigns and simulations. Section II presents the models used to specify the natural environments along a series of typical EOR trajectories. It also details the numerical simulations used to assess solar cell degradation, on one hand, and to estimate SEE on integrated electronics on the other hand. Finally, it describes two experimental campaigns conducted to measure the degradation of electronics on one hand, and the occurrence of surface electrostatic discharges on the other hand. Section III details and comments the results. Finally, Section IV discusses the key points learnt from this study.

II. EOR Mission Analysis Tools

The environment specification is performed coupling an orbit generator and space environment models of the Earth radiation belts, see sections A and B. The model developed for the estimation of solar cell degradation is presented in section C. The experiments conducted on optoelectronics components irradiated by EOR-like proton fluxes are described in section D. Section E present the method used to predict the single event rate of integrated electronic component. Finally, Section F describes the experimental setup used to estimate the electrostatic discharge risk at the surface of a spacecraft after EOR.

A. Orbit Generation

The transfer to geosynchronous orbit strongly depends on the spacecraft and on the propulsion technology. Several strategies have been identified. Spacecraft injection in the classical Ariane elliptical GTO involves a low altitude perigee at around 250 km and an apogee at the target GEO orbit. GTO^- is the sub GTO orbit with a low altitude perigee and an apogee lower than GEO. GTO^+ is GTO with higher perigee. Finally, the super synchronous transfer orbit (SSTO) is a very elliptic injection orbit with an apogee higher than GEO, and with a revolution period larger than GEO orbit. We have developed an orbit generation tool to compute simplified transfers from elliptical to circular orbit. It assumes a transfer in two steps:

- Correction of the semi-major axis with low thrust vector co-linear with velocity vector to get the semi-major axis of the targeted orbit, *i.e.* Earth radius plus GEO altitude (42164 km).
- Correction of the eccentricity with low-thrust vector perpendicular to the eccentricity vector (i.e. perpendicular to the apsides line) to get a null eccentricity at GEO.

This orbit control law is not optimal but it is sufficiently representative of GTO transfers to get good estimates of the transfer duration and ΔV. The performance calculations presented in this paper are based on launcher hypotheses derived from the characteristics of the Ariane 5-ME (a now abandoned enhancement of Ariane 5):

- it is assumed the launcher is capable of inserting a reference payload mass of 24766 kg in LEO at an altitude of 250 km.
- the launcher's upper stage (which is responsible for the final burn for orbit insertion) has a 6000 kg dry mass and is equipped with a cryogenic upper stage with a vacuum I_{sp} of 462 s (corresponding to the Vinci cryogenic upper stage, which is also the one of the upper stage of the future Ariane 6 launcher).

The payload mass inserted to a given transfer orbit is estimated by first computing the velocity increment (ΔV) of a Hohmann transfer between the reference 250 km altitude circular LEO and the considered transfer orbit (both orbit being considered as being in the same orbital plane). The propellant mass needed to perform this transfer with the launcher's upper stage is computed using the rocket equations (assuming impulsive maneuvers).

Then, the estimated payload mass inserted in the transfer orbit is obtained by subtracting this propellant mass and the upper stage dry mass (6000 kg) the reference payload mass (24766 kg).

In the frame of this study, the payload mass inserted in the transfer orbit by the launcher is a geostationary satellite platform equipped with either a chemical or an electric propulsion system, with the following hypotheses:

- For chemical propulsion platform: hydrazine propulsion system with an I_{sp} of 320 s. Propellant consumption for the transfer to GEO is calculated considering impulsive burns (use of the rocket equation).
- For all-electric platforms: electric propulsion system with an I_{sp} of 2000 s or 3500 sand a thrust to weight ratio (T/W) of 10^{-4} or 10^{-5}. Propellant consumption for the transfer to GTO is calculated through our simplified low-thrust simulation tool, considering the continuous thrust orbit transfer scheme described previously.

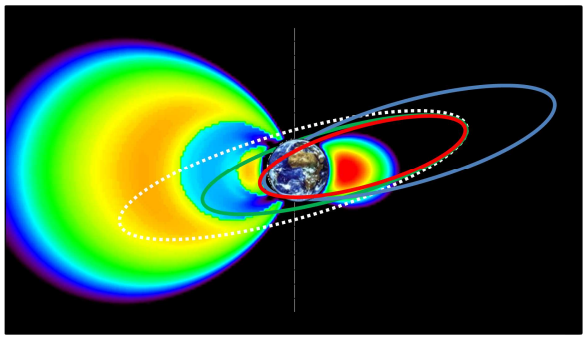

Figure 1. Schematics of orbital injections of GEO satellites (red: GTO, green: GTO+, blue: SSTO) plotted with fluxes of high energy electron (left part) and proton (right part) trapped in the radiation belts

Eventually, the mass inserted into GEO is obtained by subtracting the propellant consumed for the orbit transfer to the estimated initial mass that is inserted into the transfer orbit by the launcher. This mass inserted into GEO can be assimilated to the payload mass of the complete system, as it represents the total dry mass that can be put in GEO

by the association of the launcher (as defined above) and the platform propulsion system (which is either a chemical or an electric propulsion system). Actually, part of this dry mass include the thruster(s) and the propellant tank masses, which are not part of the "payload" as such, but this "payload mass" gives a common ground to compare the performance of different types of geostationary satellite platforms (chemical or all-electric) and different orbit transfer strategies, considering the same launcher.

The injection orbits are schematically represented in Figure 1. The impact of trapped particles depends of course on the chosen strategy since the time spent within the radiation belts, especially the Inner belt and the slot region.

B. Radiation Dose Specifications

Radiation environment specifications along the transfer orbit and at GEO are estimated for the various scenarios considered in the previous section. First of all, the radiation dose during transfers to GEO orbit is mainly due to fluxes contributions from energetic species: electrons and protons trapped into the radiation belts and protons during solar flares. Those fluxes are simulated along trajectories with AE8 and AP8 models running on the OMERE software.

The simulations were performed with the following parameters:

- GEO and GTO trapped electron environment simulated with AE8 max
- GEO and GTO trapped proton environment simulated with AP8 min
- Step size of 500 s in order to ensure more than 170 points per day
- OMERE version 5.0

C. Solar Cells Degradation

The solar cells degradation considered in this work comes from defects generated by electrons and protons interacting with active semiconductor materials. The generated defects contribute to a recombination current in the junctions of the cells. This parasitic current degrades the cells efficiency. In the frame of EOR, we estimated the impact of this technology on the end-of-life solar cells performance. For that, we used the MC-Solar code[8] which allows calculating the current-voltage characteristics of triple junction solar cells at light. For that, it is necessary to describe, on one hand, the different active layers constituting the cell in terms of optical and electrical properties and, on the other hand, the fluences of electrons and protons impacting the surface of the cell.

The degradation model relies on the law describing the minority carriers diffusion length in each material constituting the three elementary junctions:

$$L = \sqrt{D.\tau} \quad \text{with} \quad \frac{1}{\tau(NIEL,\emptyset)} = \frac{1}{\tau_0} + V_{th}.\sigma.k(NIEL).fluence(NIEL)$$

where D is the diffusion coefficient, τ is the minority carriers lifetime (τ_0 its initial value), V_{th} the thermal velocity, $\sigma.k(NIEL)$ the product of the dominant recombination centers capture cross and generation term[14], and $fluence(NIEL)$ the fluence of particles of a given Non-Ionising Energy Loss (NIEL) value. The I(V) current voltage curves of the triple junction cells under a 1 AM0 light spectrum are then calculated by solving the equations of carrier generation coming from photons absorption, and carriers transport across the structure. The equations system is solved in a 1D triple junction typical cell structure (GaInP/GaAs/Ge of type "GAGET 1").

D. Noise on Image Sensors

This part presents the method used to measure the electrical degradation of an optoelectronic imager submitted to EOR conditions. Both total ionizing dose (TID) and displacement damage dose (DDD) are able to degrade the devices. Although the TID can be simply simulated by cobalt 60 irradiation for ground testing, the DDD needs to irradiate the device with high energy proton accelerators. The electron contribution on the DDD for the EOR environment can be neglected. In the special case of imagers, the main effect of the dose (both TID and DDD) is an increase in the dark current. It corresponds to the generation of a parasitic signal on the images, reducing the dynamics and the signal-to-noise ratio. Moreover, due to some statistical discrepancies in the energy deposited by the incident particles from one pixel to another, this degradation is not homogeneous over the pixel array. A tail in the dark current histogram (also called DCNU for dark current non uniformity) appears for highly degraded pixels.

Some extreme degradations (hot pixels) are very penalizing for the mission, especially for star trackers in charge of sensing the attitude of the satellite. A single or several particle energies are generally applied during ground test campaigns. The applied fluence is computed from the incident spectrum and the non-ionizing energy loss (NIEL) of protons in the considered semiconductor.

The particularity of the present experiment is to apply an entire proton spectrum at device level. To reach this objective, the EOR proton spectra impacting the component have first been computed considering the transport of protons through shielding using the OMERE software. For a typical star tracker, the shielding is mainly achieved by the lens whose equivalent aluminum thickness is estimated to ~10 mm. Then, an irradiation campaign took place in the cyclotron accelerator of the Kernfysisch Versneller Instituut (KVI Groningen, the Netherlands). The primary energy was around 185 MeV. The final spectra are obtained by degraders that transform the primary monoenergetic beam into distributed energy spectra at device location. The beam degradation was computed thanks to an experimental simulator provided by the Centre National d'Etudes Spatiales (CNES) and by the French company TRAD. The irradiated device was a *e2v Saphirre* imager which is composed of a 1280 x 1024 pixel array (1.3 Mpixels). The pixel pitch is 5.3 µm. Each element is a 5T architecture of pinned photodiodes that enables both rolling and global shutter modes. The output signal of each pixel was digitized by 10 bit column analog to digital converters (ADCs). The protection window of the sample was removed before irradiation in order to avoid any spectrum distortion and the irradiation was performed at normal incidence. Thus, the proton spectra impacting the imager correspond to the spectra computed after the computed window shielding.

E. SEU on Nanoscale Electronic Components

Space radiation fields induce critical concerns in satellites as Single Event Effect (SEE) induced by particles. These last ten years, multi-scales modeling and physics-based Monte-Carlo or analytical approaches have been developed to address risk assessments in operational conditions and system qualifications. All-electric telecom satellite missions imply to investigate SEE risks during the in-orbit propulsion phase.

In the point of view of modeling, the nano scale induces some emerging problematic which require more detailed physical descriptions. For example, nano scale technologies are sensitive to direct ionization of protons. This problematic is critical for the space environment and questions the standard risk assessment methodology and guidelines. Moreover, the ground testing with low-energy protons seems imperative for these technologies leading to the needs for adapted facilities. The important question is to assess this risk while considering the operational environment such as structures and shielding.

MUSCA SEP3, initiated in 2007, proposes a complete simulation from the radiation fields properties, the interaction of radiation particles with the matter to the occurrence of the SEE (mainly SET, SEU/MBU and SEL) in the integrated circuit. A complete description is reported in previous works[7,15,16]. The space radiation field descriptions can be composed by protons, heavy ions and electrons, including quiet solar period and solar flare events. Carrier density morphologies induced by primary or secondary ionization in semiconductor materials are considered thanks to nuclear and ionizing databases generated by GEANT4[7]. It is necessary to consider effects due to the morphology of 3D charges due to charge deposits which become greater than the size of these scales (demonstrated for heavy ions)[17], and the effects due to direct ionization of light particle (i.e. protons and muons)[18]. Thus, 3-dimensionnal electron-hole density along primary or secondary ion particle trajectory can be described. Transport and collection models at semiconductor level are developed using TCAD simulations and allow calculating charge levels or transients induced by radiations. Moreover, impacts of the bias voltage, the layout and the fabrication processes are taken into account. To model the circuit, we describe the active zones (drains and sources), passivation and metallization layers.

We have investigated the SEU risk considering the in-orbit propulsion phase during EOR to GEO. Moreover, impacts of taking into account the direct ionization of protons and shielding conditions are investigated for a 28-nm FDSOI technology. More precisely, a 6T SRAM memory based on 28-nm FDSOI technology was considered, implying to detail the box characteristics, *i.e.* its implantation and its thickness.

Several shielding environments were considered, three uniform shielding (3mm, 1cm and 3cm) and a not uniform shielding (one axis with 3mm of aluminum, while the others with 3cm). Moreover, a fifth case considers a bare circuit.

F. Dose Effects on Surface Charging and ESDs

Charging on the external surface of a spacecraft is generated by the collection of keV to tens of keV electrons generated during geomagnetic storms or substorms. Absolute charging levels down to -8 kV to -10 kV have been reported on many GEO satellites[19,20,21] in eclipse and at GEO. At Sun, the emission of electron by photon impact (photoemission) strongly mitigates the negative charging to -500 to -2000 V typically. Differential charging of a few hundred of volts develops at the surface of covering insulators (thermal blankets, solar reflectors, solar cell cover glasses) and regularly results in electrostatic discharges (ESDs). ESD triggering is however a micron scale process. One can suspect material ageing produced during the long duration EOR transfer to GEO to modify the material properties and the threshold for ESD occurrence.

An experimental campaign has been performed in the SIRENE facility at the ONERA Toulouse Center. The background pressure was at 10^{-6} mbar. Figure 2 presents schematics of the sample assemblies. The region of interest (ROI) is the junction between a conductive surface, an insulator and vacuum. This junction is known as triple point (TP). The samples are similar to those tested during a previous work[22]. They are composed of a 127 µm thick insulating sheet made of Teflon® FEP adjusted on top of another FEP surface coated with 50 nm of silver. A hole is performed in the top insulating sheet to get a silver cathode of dimensions 20 mm × 2 mm. The silver cathode was electrically bounded to a metallic substrate biased to a voltage V_{bias} through the capacitance C_{bias} of 1 nF. This capacitance is representative of the capacitance of a spacecraft with respect to its environment. A shield has been located around the ROI to avoid the occurrence of ESDs elsewhere than in the ROI itself. Figure 3 presents the three samples used in this study, with their common shield composed of a 3 mm aluminum plate with 30 mm holes performed around the ROIs. The shield was electrically decoupled from the ground by four resistor components 20 kΩ each in order to avoid electrical arcing between the samples and the tank ground.

The samples have been exposed to a VUV deuterium source with lines at 120 and 160 nm. Materials impacted by VUV photons emit electrons with energy of a few eV. The photoelectron current density has been measured by 30 × 20 mm thin copper plates located close to the 3 samples, as represented in Figure 3. The current was about 1 nA/cm^2 representative of Earth orbits conditions. This current generates a positive differential voltage of the insulators with respect to the underlying cathode. The insulator surface potential was measured by a contactless Kelvin probe. The detailed characteristics of ESDs was measured with a Pearson current probe and with a high voltage probe controlled by an oscilloscope. ESDs have been observed with a video camera to check their occurrence time and location. Four faraday cups have been located around the samples, both to measure the flux of 400 keV electrons during exposure to radiations and to detect the occurrence of electrostatic discharges over several hours.

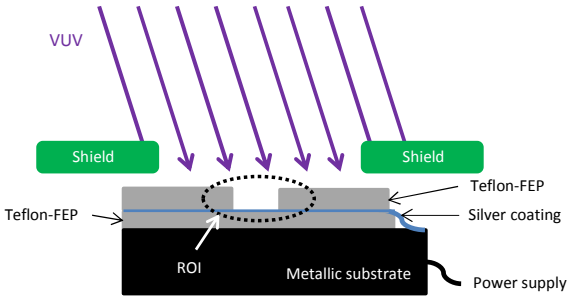

Figure 2. Schematics of the samples used to generate electrostatic discharges.

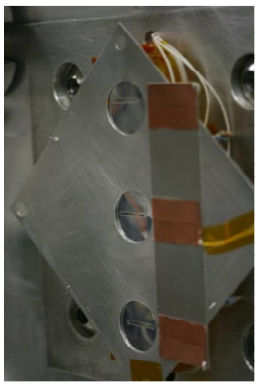

Figure 3. Picture of the three samples located inside the SIRENE facility.

The experimental protocol was composed of:

1. Bulk conductivity measurements of the virgin insulators, which consisted in:
   - bias the cathodes to -500 V
   - expose the samples to VUV during 2 minutes
   - measure the potential decay after stopping the VUV source
2. Determination of ESD threshold of virgin samples, which consisted in:
   - bias the cathodes to -500 V

- expose the samples to VUV during 10 minutes
- increase the bias voltage by -100 V each 10 minutes
- accumulate statistics

3. In order to assess the effect of penetrating electrons and subsequent radiation induced conductivity, we have repeated the previous step (ESD threshold) exposing the samples to 400 keV electron with current densities representative of the variability of the electron fluxes above 200 keV at GEO:
   - 0.1 pA/cm^2 during 30 minutes
   - 1 pA/cm^2 during 30 minutes
   - 10 pA/cm^2 during 30 minutes
4. Bulk conductivity measurements of the insulators after low dose levels of step 3
5. EOR Ageing of samples. In order to dissociate ageing and charging processes, it was chosen not to stock electrical charges within the insulator thickness during ageing, which was allowed by using the 400 keV electron beam of the SIRENE facility
6. Bulk conductivity measurements of the insulators after EOR dose level of step 5.
7. Determination of ESD threshold of aged samples

G. Dose Effects on Internal Charging and ESDs

This study was also dedicated to the characterization of possible risk of charging during the electric orbit raising. High energy electrons met in radiation belts during EOR can penetrate the outer skin of the spacecraft and accumulate in insulating materials such as cables and ungrounded conductors and cause internal electrostatic charging. If the induced electric field is sufficiently high, we have to cope with the initiation of electrostatic discharges on inner elements that can result in permanent damage to the dielectric, component failure, and phantom commands causing uncontrolled behaviour of the spacecraft

It is therefore important to test elements considered as risk in representative electron environment and assess the charging behavior and any risks of electrostatic discharges in this environment.

This task has been performed in the GEODUR irradiation test facility installed at ONERA, Toulouse, France. GEODUR is a radiation test facility allowing the study of satellite internal and surface charging, evaluation of Radiation Induced Conductivity (RIC) of thick materials and sample radiative ageing using 400 keV to 2.5 MeV monoenergetic electrons. It is equipped with a 2.5 MeV Van de Graaff electron accelerator and a double scattering system for the production of a distributed electron spectrum in the energy range [200 keV – 1 MeV]. It is instrumented with a contact-less electrostatic probe and current measurement systems for the characterisation of internal charging behaviour of space elements. The temperature of the sample holder can be controlled in the range [-180 °C, +250 °C] allowing to reproduce the temperature variations of materials on flight. A pumping system allows experiments at vacuum of around 10^{-6} hPa. This facility is equipped so as to reproduce a distributed spectrum close to the GEO electron spectrum (see Figure 4). This electron spectrum is adjustable in flux so as to get as close as possible to the required environment spectrum for material characterisation. This facility has been used in this study especially for the characterisation of ETFE cables and printed circuit board in representative EOR electron irradiation behind shielding (in an energy range between 200 keV and 1 MeV).

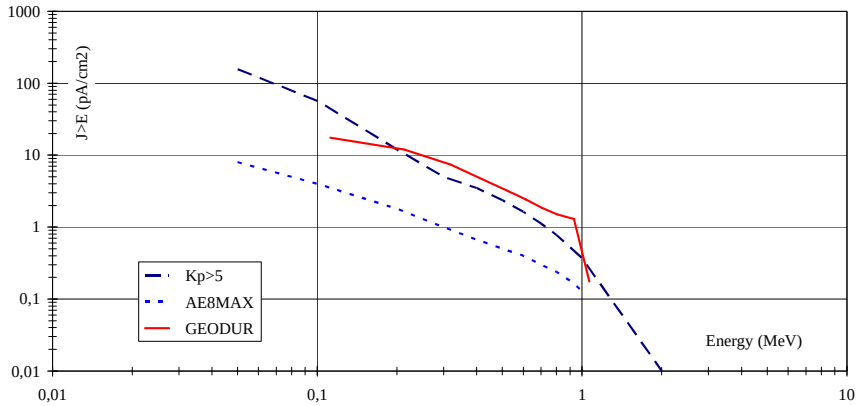

Figure 4. GEODUR electron spectrum compared to GEO AE8 max and Kp>5 spectra

Figure 5. View of the GEODUR facility

Irradiation test conditions

The samples have been irradiated with an electron spectrum representative of maximum spectrum (in regard of electron flux) met during the EOR behind 1 mm shielding for the SSTO mission with T/W = 10^{-5}. Four irradiation steps have been applied: each step is composed of 5 h irradiation and 19 h relaxation (no irradiation). This configuration is representative of the fluctuation of the electron flux met during the EOR, as we can see in Figure 6. During the experiments, in-situ measurements on the induced surface potential have been performed on the different irradiated samples.

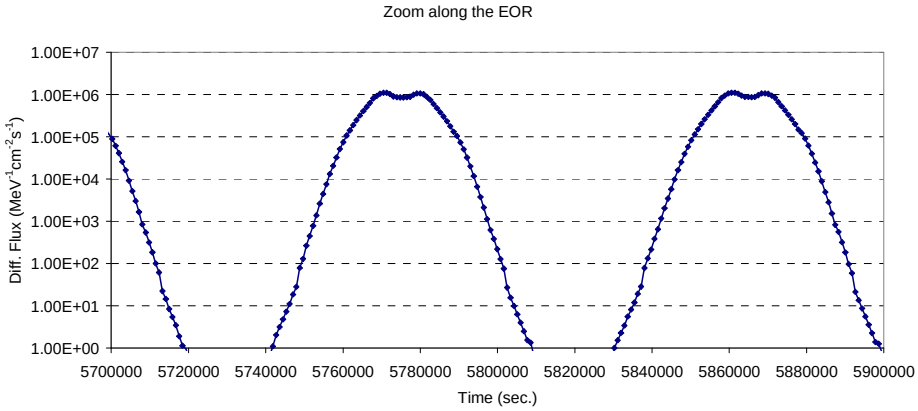

Figure 6. Evolution of electron flux at 2 MeV on a part along the EOR for the SSTO mission

Irradiated test samples

Two different samples have been irradiated:

- A space used printed circuit board (PCB): this PCB was a multilayer PCB with internal metallic plan connected to ground in our experiments. This PCB is composed of metallic tracks at the surface that were left at floating potential during the experiments. Around ten floating tracks have been connected to a circular metallic flag which allows measuring the surface potential built up on these tracks during irradiation, using a non-contact Kelvin probe that moves along the sample and scans the flag and the free surface of the PCB.
- ETFE wires: ETFE is widely used for inner cables. The sample is composed of a sheet of several 5 cm long piece of wires so as to produce a significant surface area for the electric potential measurements.

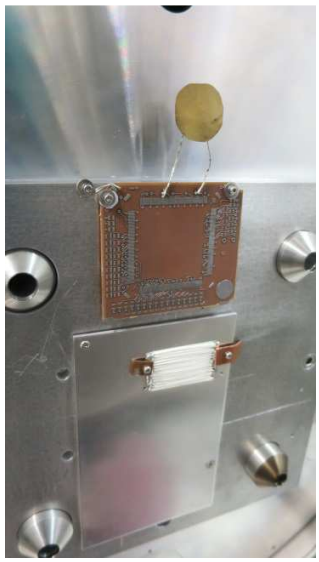

Figure 7. View of the PCB and ETFE wires tested in the GEODUR test facility

III. Results

In this part, we describe the GTO, GTO+ and SSTO EOR trajectories obtained from our orbit generator and the corresponding radiation specifications in Sections A and B, respectively. Solar cell degradations are presented in Section C for all missions. Section D and E focus on the effect of GTO EOR mission. Section D addresses the noise generated on image sensors. Section E estimates the rate of single event upsets on nanoscale electronic components. Section 0 presents the effects of EOR missions on surface dielectric charging and discharging.

A. Orbit Definition

Three GTO injection orbits have been compared using electrical propulsion parameters T/W of 10^{-4} and 10^{-5}:

- GTO trajectory : 250 km × 35786 km, representative of the initial orbit of Eutelsat 172B launched by Ariane 5.
- SSTO trajectory : 250 km × 60000 km, representative of the initial orbit of Eutelsat 115 West B, ABS 3A launched by Falcon 9.
- GTO+ trajectory : 5000 km × 35786 km, which is an alternative to the two launch strategies listed above.

Their durations are compared to the classical chemical injection orbit (250 km × 35786 km) in Table 1. EOR spacecraft spend between 22 and 28 days and between 218 and 282 days to reach GEO with a thrust to weight ratio of 10^{-4} and 10^{-5}, respectively. Figure 8 compares the altitude as a function of time of GTO, SSTO and GTO^{+} transfers for T/W = 10^{-5}. It also presents the trajectories of the two BOEING all-electrical telecom satellites launched in 2015 which are well represented by the SSTO scenario computed in this work. The trajectory points are available at obtained from Two Lines Element Sets (https://www.celestrak.com/NORAD/elements/. The satellites were injected at a perigee of about 250 km and an apogee above 60 000 km. The first phase of the mission consisted in increasing both apogee and perigee. The second phase consisted in circularizing the orbit, decreasing the apogee and increasing the perigee. The satellites launched in June 2017 (Eutelsat 172 B and Viasat-2) have been injected in a GTO orbit at around 200 km with an apogee at GEO.

Table 1 – Results for the transfer to GEO for all EP missions using various orbit transfer scenarios and considering two I_{sp}, compared to classical chemical propulsion. Durations are expressed in days.

I_{sp} = 2000s							
Transfer strategy	**GTO**			**SSTO**		**GTO+**	
Propulsion system	Chemical Isp=465 s	EP Isp=2000 s T/W = 10^{-4}	EP Isp=2000 s T/W = 10^{-5}	EP Isp=2000 s T/W = 10^{-4}	EP Isp=2000 s T/W = 10^{-5}	EP Isp=2000 s T/W = 10^{-4}	EP Isp=2000 s T/W = 10^{-5}
Duration (days)	1.6	28	282	25	251	22	218
Thrust (N)	-	11.8	1.2	10.8	1.1	10.3	1.0
Power (kW)	-	115.5	11.5	105.8	10.6	100.8	10.1
Initial mass (kg)	12000	12000	12000	10991	10991	10479	10479
Final mass (kg)	7508	10624	10625	9861	9863	8777	8782
Propellant mass (kg)	4492	1376	1375	1130	1128	1702	1697
I_{sp} = 3500s							
Transfer strategy	**GTO**			**SSTO**		**GTO+**	
Propulsion system	Chemical Isp=465 s	EP Isp=3500 s T/W = 10^{-4}	EP Isp=3500 s T/W = 10^{-5}	EP Isp=3500 s T/W = 10^{-4}	EP Isp=3500 s T/W = 10^{-5}	EP Isp=3500 s T/W = 10^{-4}	EP Isp=3500 s T/W = 10^{-5}
Duration (days)	1.6	28	282	25	251	22	218
Thrust (N)	-	11.8	1.2	10.8	1.1	10.3	1.0
Power (kW)	-	202.1	20.2	185.1	18.5	176.5	17.6
Initial mass (kg)	12000	12000	12000	10991	10991	10479	10479
Final mass (kg)	7508	11193	11193	10331	10332	9928	9929
Propellant mass (kg)	4492	807	807	660	659	551	550

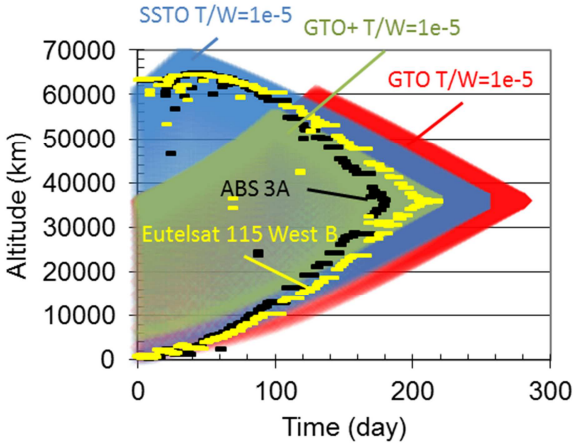

Figure 8. Spacecraft altitude during transfer to GEO assuming several EOR mission scenarios compared to actual Eutelsat 115 West B and ABS 3A trajectories

The orbit generator developed for EOR trajectories showed good agreements with current EP spacecraft practices, at least concerning duration and altitude versus time. This is thus fully relevant input for the assessment of space environment effects.

B. Radiation Dose Specifications

The average differential fluxes obtained along the seven orbits presented in Table 1 are presented in Figure 9, both for electrons and protons. They are compared to the average differential flux during the 15 years mission at GEO. Figure 10 presents the ratio between each of these fluxes and the average differential flux along the transfer orbit associated to chemical propulsion. The average EOR differential fluxes of electron below 6 MeV range between 0.5 and 1.2 times the chemical transfer average flux, pending on the chosen scenario and on the considered energy. GTO^+ exceeds GTO and SSTO by a factor of around 10 % and 30 %, respectively. The difference is more significant for protons > 10 MeV with GTO^+ exceeding GTO and GTO^+ by a factor of around 2 and up to 10, respectively. At GEO, the low energy (E< 1MeV) electron contribution is nearly the same as during transfer to GEO. At higher energy, however, the electron flux in the outer belt exceeds the flux at GEO by a factor of 5 approximately. Finally, the trapped proton contribution at GEO is negligible compared to GTO trajectories.

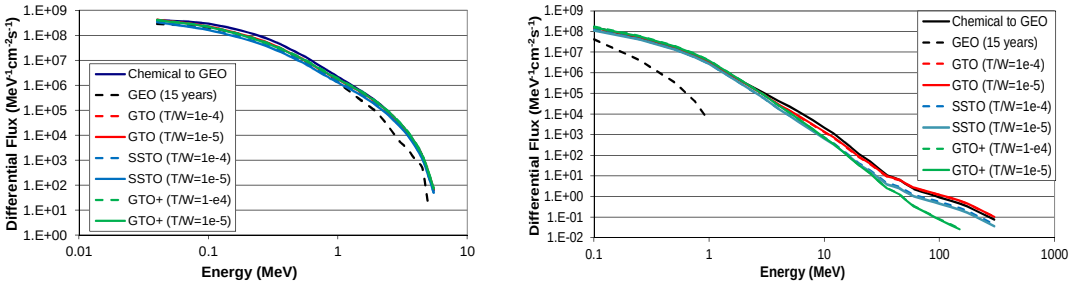

Figure 9. Electron (left) and proton (right) average differential fluxes of, assuming several scenarios for transfer to GEO, compared to the 15 years mission at GEO alone.

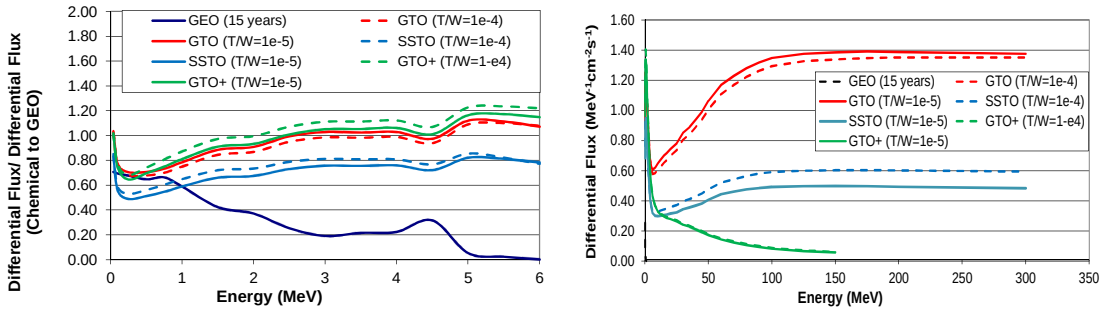

Figure 10. Ratio between the average differential flux obtained during each of the EOR transfer scenario and during chemical transfer, for electrons (left) and protons (right)

The total electron and proton fluence received by the spacecraft are plotted in Figure 11. Table 2 presents the fluence of 1 MeV electrons. The fluence is computed by multiplying the average differential flux along the orbit by the orbit duration, considering the 15 years mission at GEO and each of the transfer to GEO scenarios. The electron fluence along the EOR trajectories obtained with T/W = 10^{-5} exceeds the fluence obtained along EOR trajectories obtained with T/W = 10^{-4} EOR trajectories and the fluence obtained along the chemical propulsion trajectory by a factor of ~10 and ~100, respectively. That roughly corresponds to the additional time spent within the radiation belts; *i.e.* ~200 days instead of ~20 days and ~2 days, respectively. Assuming a T/W parameter of 10^{-5}, which is representative of current spacecraft capabilities, the fluence over the 6-7 months transfer to GEO is ~5% to ~10 % the fluence over 15 years at GEO. The transfer by electrical propulsion represents thus a non-negligible contribution to the total dose received during the full mission duration. The proton fluence during T/W = 10^{-5} EOR missions exceeds by orders of magnitude the fluence during 15 years at GEO and by a factor up to 200 the fluence during 2 days GTO by chemical propulsion.

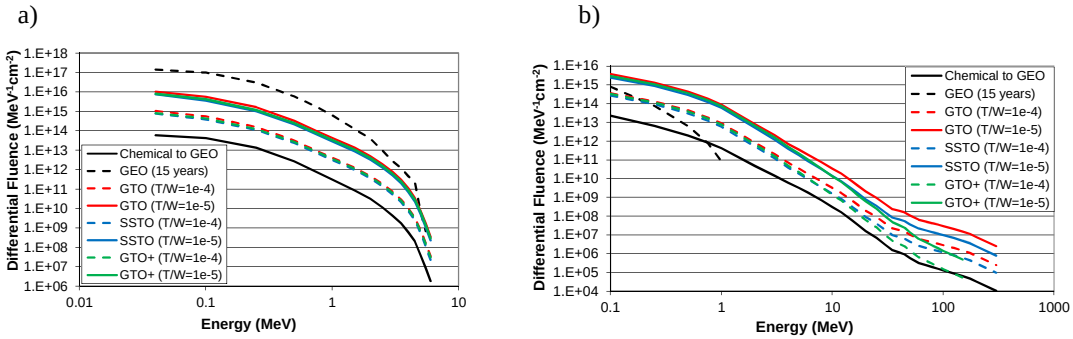

Figure 11. Differential fluence of (a) electrons and (b) protons under the same conditions as in Figure 9.

Table 2 – 1 MeV electron fluence during GTO using various orbit transfer scenarios. Fluence values are expressed in 10^{12} × $MeV^{-1}.cm^{-2}$.

Mission	Chemical GTO	EP GTO T/W = 10^{-4}	EP GTO T/W = 10^{-5}	EP SSTO T/W = 10^{-4}	EP SSTO T/W = 10^{-5}	EP GTO^{+} T/W = 10^{-4}	EP GTO^{+} T/W = 10^{-5}
Fluence	0.3	4.0	41	3.0	14	3.6	17

Finally, Figure 12a presents the total dose received during the 15 years at GEO and during the different scenario of transfer to GEO by electrical and chemical propulsion. The dose profile is represented as a function of aluminum equivalent shielding thickness. For thicknesses lower than 1mm, the dose is mainly due to energetic electrons. However, the Bremsstrahlung electron contribution increases with the thickness. In conclusion to this radiation dose specification part, the dose is normalized by the total dose received after 15 years in GEO. Figure 12b represents the ratio of dose received during the transfer orbit over the dose received during the 15 years mission. The transfer duration represents respectively for chemical, and for electrical GTO (T/W= 10^{-4}) and GTO (T/W=10^{-5}) propulsion, 0.04%, 0.4% and 4% of the 15 years mission duration and induces around 0.1 %, 1% and 10 % of the total dose at the end of the mission. Current electrical thrusters allows a T/W of around 10^{-5}, which means that the dose received by spacecraft after a GTO duration of about half a year is around 10% of the total dose. Table 3 finally presents the total dose received at 5 mm of aluminum equivalent shielding. An extra 15 to 20 krad is added by EOR with respect to classical chemical propulsion transfers.

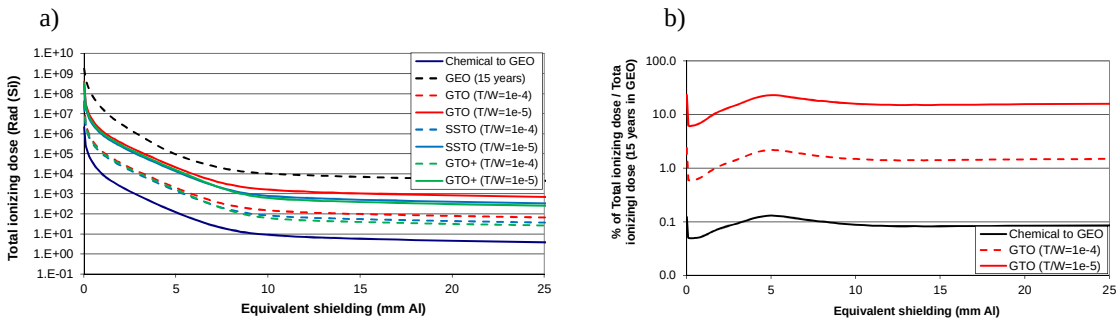

Figure 12. (a) Total ionizing dose received during transfers to GEO compared with the total ionizing dose received during 15 years at GEO and (b) Total dose received during the transfer to GEO by chemical propulsion and by two electrical propulsion scenarios, in % of the dose received during the 15 years mission at GEO

Table 3 - Calculated ionizing dose at 5 mm equivalent aluminum, for all EP missions using various orbit transfer scenarios. Dose values are expressed in kRad (Si).

Mission	GEO only	GTO T/W = 10^{-4} & GEO	GTO T/W = 10^{-5} & GEO	SSTO T/W = 10^{-4} & GEO	SSTO T/W = 10^{-5} & GEO	GTO^{+} T/W = 10^{-4} & GEO	GTO^{+} T/W = 10^{-5} & GEO
TID	90.8	92.8	110.9	92.2	104.7	92.4	106.0

C. Solar Cell Degradation

The GAGET 1 solar cell degradation during GTO has been estimated for the different scenarios presented in section III-A using the electron and proton fluences presented in section B.

The solar cell performance parameters reached at the end of the transfer to geosynchronous orbit are presented in Table 4. V_{oc} is the open circuit voltage. I_{sc} is the short circuit current. P_{max} is the maximum power. The power loss is the difference between the initial value of P_{max} and the value of P_{max} after the transfer. The solar cell degradation is negligible during GTO by chemical propulsion and reaches a maximum value of 2.6% for the GTO scenario assuming T/W = 10^{-5}. The SSTO and GTPO+ scenarios involve a degradation of 1.2 % and 2.0%, respectively, assuming T/W = 10^{-5}. Increasing T/W up to 10^{-4} decreases the degradation by a factor of around 4 to 6 with respect to scenario with T/W of 10^{-5}.

Table 4 - Calculated solar cell parameters and performance during GTO using various orbit transfer scenarios. V_{oc}, I_{sc} and P_{max} values are expressed in % of their initial value. The power loss values are expressed in % of the initial value of P_{max}.

Mission	Chemical GTO	EOR GTO T/W = 10^{-4}	EOR GTO T/W = 10^{-5}	EOR SSTO T/W = 10^{-4}	EOR SSTO T/W = 10^{-5}	EOR GTO^{+} T/W = 10^{-4}	EOR GTO^{+} T/W = 10^{-5}
V_{oc}	100,0	100,0	98,8	100,0	99,6	100,0	98,8
I_{sc}	100,0	100,0	100,0	100,0	100,0	100,0	100,0
P_{max}	100,0	99,6	97,4	99,7	98,8	99,7	98,0
Power Loss	0,0	0,4	2,6	0,3	1,2	0,3	2,0

Table 5 presents the end-of-life solar cell degradation assuming several scenarios for GTO and a 15 years mission at GEO. The 15 years GEO mission alone is responsible for a degradation estimated to 11.4 %. Using the chemical propulsion does not lead to extra degradation. The electrical propulsion scenarios induce an additional decrease in the EOL power of 0.5% to 0.7 % with T/W of 10^{-5}. The power losses of 2.6 % just after the GTO are faded into the progressive degradation that occurs during the following 15 years at GEO. The damaging process is not linear and tends to smooth the initial conditions with time spent in orbit. As a result, the key point for solar panel dimensioning is the availability of power for electrical propulsion during GTO, including early solar power degradation, rather than EOL.

Table 5 - Calculated solar cell parameters and performance during 15 years GEO missions using various orbit transfer scenarios. V_{oc}, I_{sc} and P_{max} values are expressed in % of their initial value. The power loss values are expressed in % of the initial value of P_{max}.

Mission	Chemical GTO & GEO	GTO T/W = 10^{-4} & GEO	GTO T/W = 10^{-5} & GEO	SSTO T/W = 10^{-4} & GEO	SSTO T/W = 10^{-5} & GEO	GTO^{+} T/W = 10^{-4} & GEO	GTO^{+} T/W = 10^{-5} & GEO
V_{oc}	93,9	93,9	93,9	93,9	93,9	93,9	93,9
I_{sc}	99,7	99,7	99,7	99,7	99,7	99,7	99,7
P_{max}	88,6	88,6	87,9	88,6	88,1	88,6	88,0
Power Loss	11,4	11,4	12,1	11,4	11,9	11,4	12,0

D. Noise on Image Sensors

Figure 13 presents the proton differential flux impacting the external surface of the protection lens of the image sensor and the proton differential flux that goes through the 10 mm equivalent aluminum shielding of this lens to finally impact the sensor. In this paragraph, we assumed a GTO transfer by electrical propulsion with a parameter T/W of 2×10^{-5}. It corresponds to a total duration of 141 days, i.e. reduced by one half with respect to GTO trajectory that assumed T/W of 1×10^{-5}. The unshielded initial flux, in red, decreases from more than 10^{8} $cm^{-2}s^{-1}MeV^{-1}$ at 0.1 MeV to around 1 $cm^{-2}s^{-1}MeV^{-1}$ at 100 MeV. After the shield, in blue, a maximal flux of a bit more than 1 $cm^{-2}s^{-1}MeV^{-1}$ is obtained at around 20 MeV. The effect of shielding is negligible above 200 MeV. Figure 14 presents the total proton fluence during EOR GTO, in blue. This computed fluence is the shielded average flux multiplied by the duration of the GTO phase. The fluence applied during the experimental campaign is plotted in pink. The applied flux fits the expected flux up to 180 MeV.

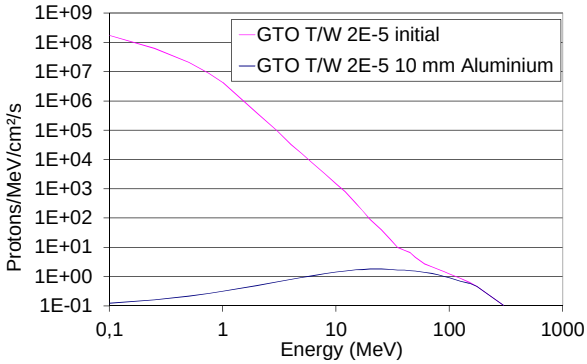

Figure 13. Average proton flux along the EOR GTO T/W = 2×10^{-5} scenario (in pink) and corresponding flux across 10 mm thick aluminum (in blue)

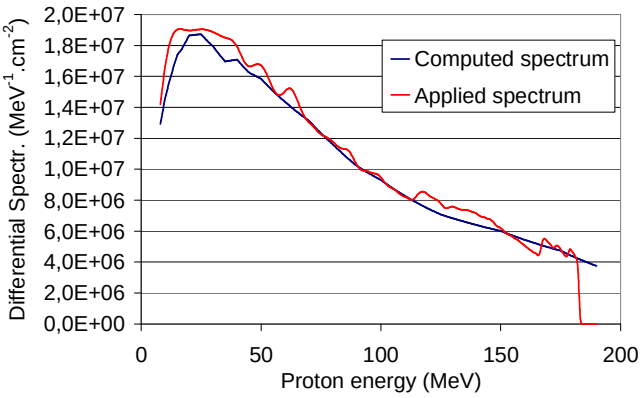

Figure 14. Comparison between the proton fluence representing the GTO EOR mission (referred as computed) and the fluence actually applied during the experimental campaign.

Figure 15 presents the histograms of the increase in the dark current due to irradiation. For each pixel, the digital output signal of the imager is a number given in unit of least significant bit (lsb) between 0 and 1023 in the case of this 10 bits imager. The dark current corresponds to the output of the pixel in darkness divided by the exposure time. It is given in unit lsb/s. Pixel with significant damages produce high levels of lsb/s. Measurements have been done before and one month after the proton irradiation, at room pressure and temperature. The initial dark signal was close to zero. After exposure, some pixels exhibited a large degradation. The red curve in Figure 15 shows the differential histogram of dark signal increase. It gives the number of pixels with a given dark current increase after exposure to EOR radiations. The blue curve in Figure 15 shows the number of pixels with a dark current increase above a given value. More than 4,000 pixels (0.3 % of the total number of pixels) have an increase above 100 lsb/s and the extreme values reach a few thousands of lsb/s. To build a precise picture, the required exposure time of a sensor is typically 10 to 100 ms. As a result, after EOR, 4000 pixels will present a dark signal corresponding to around 1 to 10 digital units. 200 pixels will exhibit degradation between 10 and 100 digital units. For applications such as star tracker, in charge of attitude control, this represents thus a concern to be addressed.

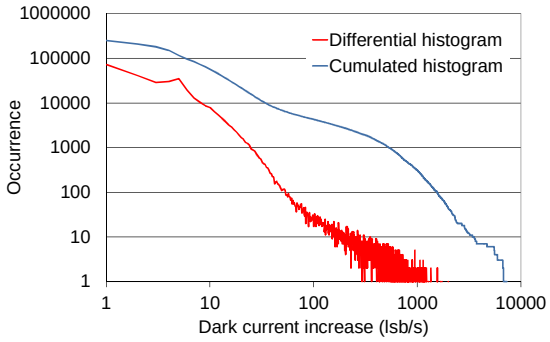

Figure 15. Differential and cumulative histograms (with a bin of 1 lsb/s) of the dark current increase at 300 K and after proton irradiation representative of a 140 days EOR GTO mission.

E. SEU on Nanoscale Electronic Components

Figure 16 presents (a) the nuclear and (b) the direct ionizing proton SEU cross sections obtained by MUSCA SEP3 calculations and considering several shielding conditions (∅, 3 mm, 1 cm, 3 cm uniform shielding and no uniform shielding). Concerning the ionization process, the increase of the shielding induces a shift of the cross section peak towards high energies. The spreading of this peak, i.e. energy range, is a very important parameter because directly related to the radiation field “efficient energy range”. In other words, as this energy range is shifted

towards high energies, the impact on SER is attenuated. Nuclear cross section threshold are shifted by the shielding thickness increase. These results demonstrate the significant impact of the material environment surrounding the device. By associating these cross sections with the proton irradiation during EOR, it is possible to calculate the Soft Error Rate (SER) in SEU per second and per bit. Our analysis consists in considering proton spectra averaged over one week during the in-orbit propulsion phase, then to evaluate the SER dynamics.

Figure 17 presents the SER in number of events per hour and per device (assuming a 4 Mbit SRAM), considering (a) the nuclear and (b) the ionization processes, under the five shielding conditions. We assumed a EOR/GTO scenario with T/W of 10^{-5}. During the initial injection phase that crosses the radiation belts, the SER is significantly larger, of the order of 2 to 4 decades depending on the shielding conditions, at GEO. This is mainly due to the contribution of the direct ionization process. This means that all-electric satellite missions require a significant refinement of risk assessment methods for nanoscale technologies, combining direct ionization, 3D morphology and shielding properties. Complementary analyses show that ionization from primary protons is the preponderant contribution to the overall SEU risk, but shielding characteristics can mitigate this analysis. These results indicate clearly that for this 28-nm FDSOI technology, ionization from primary protons is the preponderant contribution to the overall SEU risk, leading to respectively around 80 and 95% for 3cm and 3mm uniform aluminum shielding assumptions. Thus, nanoscale technologies are particularly affected by direct ionization of proton process depending on the shielding conditions. Indeed, two orders of magnitude are observed in total SEU number and SER between 3cm and 3mm. Assuming a uniform shielding of 3 mm equivalent aluminium, a few SEU are expected to occur each hour during the first 3 to 4 weeks. Further assumption and/or information on SRAM geometry available from component designers will allow assessing the operational risks during the EOR phase.

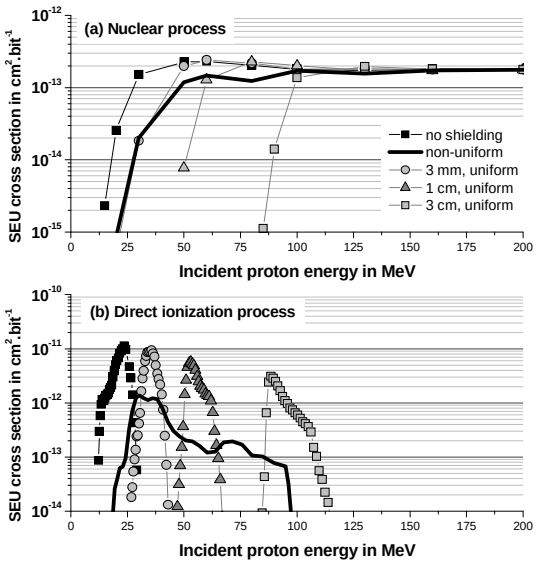

Figure 16. (a) Nuclear and (b) direct ionizing proton SEU cross section of a 28-nm FDSOI technology considering several shielding conditions (∅, 3 mm, 1 cm, 3 cm uniform shielding and no uniform shielding).

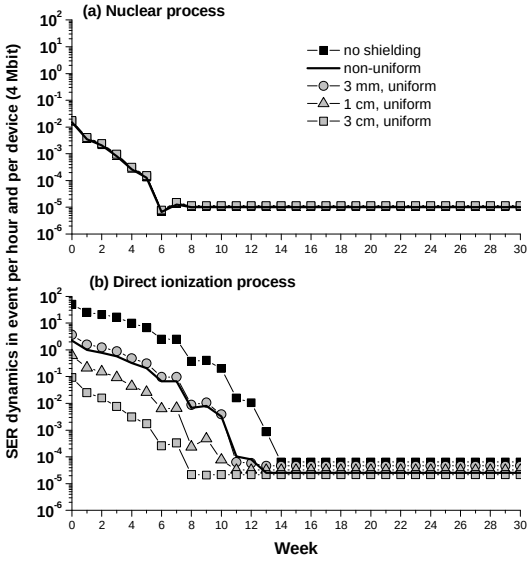

Figure 17. (a) Nuclear and (b) direct ionizing proton SER dynamics of a 28-nm FDSOI technology considering several shielding conditions (∅, 3 mm, 1 cm, 3 cm uniform shielding and no uniform shielding) and all-electric telecom satellite mission.

F. Dose Effects on Surface Charging and ESDs

This section describes the results of the experimental protocol of Section II-F. First, we present the effect of radiations on dielectric conductivity. Second, we present a typical example of ESD. Finally, the effect of dose on ESD voltage threshold and occurrence is examined.

We first performed step 1 of the experimental protocol and check that the insulator equilibrium charge was reached after 2 minutes of exposure to VUV radiation. Photoemission created a positive space charge at the top surface of the Teflon® FEP that fully counterbalanced the negative potential V_{bias} since the measured potential was close to zero. The volume conductivity of virgin Teflon® FEP is 10^{-19} to 10^{-20} $ohm^{-1}.m^{-1}$. The low dose received during the third step of the protocol (cumulated 30 minutes exposition to 0.1, 1.0 and 10.0 pA/cm^2 of 400 keV electrons) involves significant changes. The increase in the bulk conductivity at step 4, up to 10^{-15} $ohm^{-1}.m^{-1}$, is the result of delayed radiation induced conductivity. Radiation induced conductivity is the enhancement of charge carrier transfer thanks to the generation of electron-hole pairs that produces electron transfer from the valence band to the conduction band. The insulators have then been exposed to a total dose of 8×10^5 Gy representative of SSTO EOR with no shielding. It has been achieved after an exposure time of 20 hours to 400 keV electrons with a current density of 5 nA/cm^2. After step 5, the bulk conductivity increased up to 3×10^{-15} $ohm^{-1}.m^{-1}$.

The electrical signature of a typical ESD produced on a virgin sample is represented in Figure 18. It shows the evolution with time of the current flowing through the sample and of the bias potential. The current emission corresponds to a partial discharge of the capacitor C_{bias} during a few microseconds. The maximal current is 0.2 A which is one order of magnitude lower than previous experiments[22] performed with the same input parameters (V_{bias}, C_{bias}, materials). The voltage measured between the sample and the tank ground decreased from -900 V to -800 V, which means that the discharge prematurely extinguished before C_{bias} was totally discharged. Hundreds of discharges have been generated on each of the three samples. All of them conducted to the very limited discharges of C_{bias} (release of < 10 % of the stored charges). The presence of the metallic shield explains why the ESDs are partial ESDs. As the shield is floating with respect to ground through four resistors, a voltage drop occurs when the plasma expanding from the ESD site reaches the internal side of the shield. This potential drop reduces the electric field close to cathode which in turn does not sustain the discharge anymore. The duration of the ESDs, ranging from 1 to 10 µs, is representative of the time required for a plasma bubble expanding at a velocity of 10^3 to 10^4 m/s to reach the shield located at a distance of 1 cm. The setup was very efficient at generating a large number of ESDs without degrading the cathode because the energy released was limited. It allows perform statistics on the same sample all along the series of steps of the protocol.

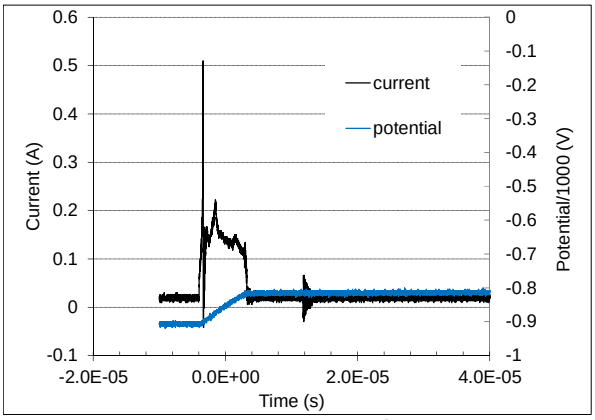

Figure 18. Electrical signal of a typical ESD produced on the test setup of Figure 2

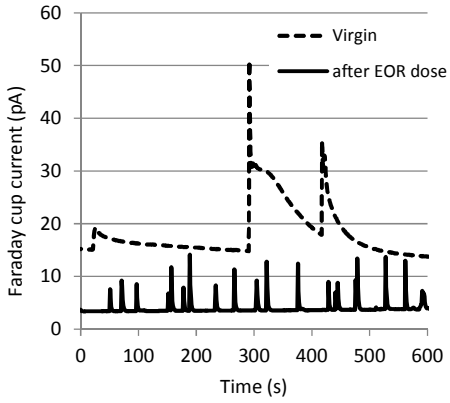

Figure 19. Time evolution of the electron current collected by faraday cups during ESD test protocol. The dashed and the plain lines have been obtained during step 2 and step 7, respectively; both at V_{bias} = -800 V.

The ESD voltage threshold for virgin samples, during step 2, ranged from V_{bias} equal to - 600 down to -800 V. During step 3, the voltage threshold ranged between -700 V and -900 V when the samples were irradiated by low currents of penetrating electrons. The voltage threshold ranged between -800 and -850 V a day after step 3. The

voltage threshold measured during step 7, *i.e.* after the samples received the EOR dose, ranged between -700 and -800 V. As a result, the voltage conditions leading to ESD occurrence did not change significantly before and after exposition to the dose received during transfer to GEO by EOR. The experiments of step 3 with dose rates representative of MEO/GEO environments, did not produce any significant change neither. Physically, it is suggested that the photoelectron current of a few nA/cm2, responsible for potential gradients building at triple point level, remains orders of magnitude larger than the current conducted through the insulator sheet. Figure 19 shows the time evolution of the current collected by the Faraday cup during step 2 and step 7 at V_{bias} = -800 V. The occurrence of tiny ESDs increased a lot after EOR ageing. Ageing probably modified the mechanical structure of the insulating tape, producing cracks and deforming the insulator shape close the cathode gap. Such effects can modify the ESD regime and influence the duration and amplitude of vacuum arcs.

This campaign shows the necessity to test the susceptibility to ESDs of sensitive parts submitted to ageing such as solar cell coupons, with possible implications on secondary arcing sustained by the solar panels.

G. Dose Effects on Internal Charging and ESDs

Figure 20 presents the evolution of the surface potential measured on the PCB (flag [metallic floating tracks] and PCB center] and ETFE wires during the four cycles of irradiation. We can clearly notice a steady rise of the surface potential on the different parts of the tested samples: charges tend then to get accumulated in the inner material up to the initiation of an electrostatic discharge. Two discharges have indeed been detected on PCB during the 3rd and the 4th cycle: we can observe a steep drop on the flag potential during these two cycles, which is the signature of an electrostatic discharge. These elements used on spacecraft might therefore be prone to be submitted to frequent electrostatic discharges during EOR. This is however important to mention that 1 mm shielding is a worst case scenario : conventional shielding is usually 3 mm which reduces the incident flux, and then the charging kinetics, by around one decade. We should however still observe a steady but slower rise of the surface potential, up to the initiation of electrostatic discharges after 30 or 40 days on flight during the EOR (which last 120 days). Finally, ETFE could be subjected to dielectric breakdown for electric fields close to the one reached in this experiment. In EOR, we could then have to cope with dielectric failures of insulating material and to the initiation of high leakage currents that could be detrimental for the on-board equipment.

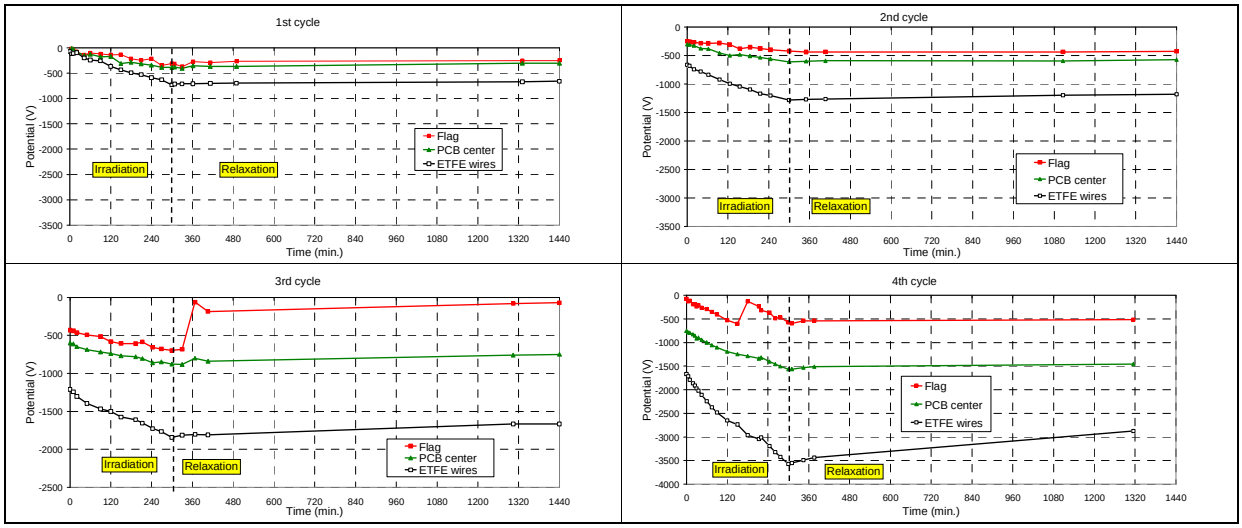

Figure 20. Evolution of surface potential on PCB (flag and center of PCB) and ETFE wires along the 4 irradiation cycles

IV. Conclusion

This paper presented a detailed analysis of additional detrimental effects that all-electric spacecraft are suspected to face during geostationary orbit raising with respect to classical propulsion missions. These effects are related to a prolonged time spent within the radiation belts. New EOR missions and targets require advanced numerical and experimental tools for the estimation of equipment reliability against the harsh space environment. Our analyses combined test campaigns and numerical simulations to estimate cumulated degradation and charging and single event effects.

The main conclusions are:

- The numerical simulations of orbit transfer scenarios provided a fair compromise between representativity of the results, computing resources and ease of use. A simplified but consistent comparison has been made between EOR scenarios and chemical propulsion. This tool perfectly fits the requirements for the assessment of space environments effects.
- Globally, EOR missions receive an extra 15 to 20 krad during transfer to GEO with respect to classical chemical propulsion missions.
- The average flux of energetic particles during GTO^+ EOR missions exceeds GTO and SSTO by a factor of around 10 % and 30 %, respectively. Even though it last longer than GTO^+, the SSTO mission receives a lower dose level because its injection apogee is above the radiation belts and because the spacecraft velocity is high when penetrating the Van Allen belts.
- The key point for solar panel dimensioning is the availability of power for electrical propulsion during GTO, including early solar power degradation of about 1 to 3% during EOR. EOL conditions are not depending on the GTO initial phase. These results would require however to be compared to available in-flight degradation observations, such as during SMART-1, in order to improve our modelling capabilities and help prepare future missions.
- Opto-electronics components used, as e.g., on star trackers are sensitive to the high energy proton fluence cumulated within the radiation belts during EOR. Spacecraft designers may need to pay attention to the increase in the dark signal current.
- Nanoscale technologies imply the use of a multi-physics approach, taking into account all physical mechanisms and refined description of material environment. A few SEUs are expected to occur each hour during the first 3 to 4 weeks on nano-scale electronic components (28 nm).
- Surface material ageing during EOR has been simulated by penetrating electrons. Even though the voltage threshold required to trigger surface electrostatic discharges remained unchanged before and after ageing, the occurrence of low energy discharges was significantly increased. It is thought that mechanical cracks and deformations occurred at the insulator surface.

Additional effects not discussed in this paper include ageing of thermal control surface material under electron, proton, VUV, and would require further testing or analysis. Future tests should also involve long thermal cycling series since hundreds of eclipses occur during EOR missions. Another important effect concerns the ESD risk in internal parts, which is the result of the accumulation of charges on thick dielectrics inside the spacecraft. It is recommended to further test coupon and electronics representative of flight configuration under flight representative conditions, in order to prepare future missions, and to use the numerical simulation tools to extrapolate to mission conditions and duration when testing is not permitted by ground facilities. In addition to cumulated dose and single event effects, one need to also consider the self-produced environments generated by EP plumes: spacecraft charging, erosion and contamination. This is the subject of a companion paper[23]. Finally, ONERA and ARTENUM are currently developing the Spacesuit(e) multi-physics software that include numerical models and tools for the assessment of natural and self-produced environments effects (ww.space-suite.com).

Acknowledgments

This work has been performed in the frame of the ORESTE and ELECTRA research projects of ONERA - The French Aerospace Lab. The authors are grateful to CNES and ESA for their continuous support on improving our experimental and numerical tools. The authors also thank ARTENUM for collaborating to the Spacesuit(e) project.

References

[1]Likar, J. J., A. Bogorad, K. A. August, R. E. Lombardi, K. Kannenberg, and R. Herschitz, "Spacecraft Charging, Plume Interactions, and Space Radiation Design Considerations for All-Electric GEO Satellite Missions", IEEE Trans. Plasma Sci., Vol. 43, No. 9, 2015.

[2]Vette, J. I., "The AE-8 trapped electron model environment", NASA-TM-107820, 1991.

[3]Sawyer, M., and J. I. Vette, . "AP8 Trapped Proton Environment for Solar Maximum and Solar Minimum", 1977.

[4]Sicard-Piet, A., S. Bourdarie, D. Boscher, H. W. Friedel, M. Thomsen, T. Goka, T. et al., "A new international geostationary electron model: IGE-2006, from 1 keV to 5.2 MeV", Space Weather, 6, S07003, 2008. doi:10.1029/2007SW000368.

[5]ECSS, "Space environment", ECSS-E-ST-10-04C, 2008.

[6]NASA, "Mitigating In-Space Charging Effects—A Guideline", NASA-HDBK-4002A, 2011.

[7]Hubert, G., S. Duzellier, C. Inguimbert, C. Boatella-Polo, F. Bezerra, and R. Ecoffet, "Operational SER calculations on the SAC-C orbit using the Multi SCAles Single Event Phenomena Predictive Platform (MUSCA SEP3)", IEEE Trans. Nucl. Sci., Vol. 56, No.6, pp. 3032-3042, Dec. 2009.

[8]Gauffier, A., J.-P. David and O. Gilard, "Analytical model for multi-junction solar cells prediction in space environment", Microelectronics reliability, 08/2008: 48 (8-9-48), 1494-1499, 2008.

[9]Sarrailh, P., T. Paulmier, B. Dirassen, D. Rodgers, G. Santin, F. Cipriani, D. Payan, "Validation Through Experiments of a 3-D Time-Dependent Model of Internal Charging", IEEE Transactions on Plasma Science, Vol 45, 9, 2017

[10]Roussel, J.-F. E. Vanhove, T. Tondu, D. Faye, and P. Guigue. "Ultraviolet Fixation of Molecular Contamination: Physical Model Numerical Implementation and Validation", Journal of Spacecraft and Rockets, Vol. 53, Special Issue on Materials in a Space Environment (2016), pp. 1159-1165. https://doi.org/10.2514/1.A33504

[11]Vanhove, E., J.-F. Roussel, V. Inguimbert, J.-P. Chardon, "UV photofixation of molecular contamination: simulation of in-flight data", Proc. SPIE 9952, Systems Contamination: Prediction, Control, and Performance 2016, 995207 (27 September 2016); doi: 10.1117/12.2238935.

[12]Matéo-Vélez, J.-C. P. Sarrailh , S. L. G. Hess and J.-F. Roussel, "Simulations of plasma thruster and large antenna effects on the electrostatic behavior of spacecraft in GEO", 14th Spacecraft Charging and Technology Conference, Noordwijk, NL, April 2016.

[13]Sarrailh, P., S. L. G. Hess, J.-C. Mateo-Velez, Th. Gineste, and M. Belhaj, Simulations of plasma thruster effect on the electrostatic behavior of spacecrafts in GEO, AIAA SPACE, Pasadena, California, 2015.

[14]Gauffier, A., J.-P. David, O. Gilard, T. Nuns, C. Inguimbert and A. Balocchi, "Experimental methods for defect introduction rates determination in multi-jonction solar cells, IEEE Trans. Nucl. Sci, 2009.

[15]Hubert, G., and L. Artola, "Single-Event Transient Modeling in a 65-nm Bulk CMOS Technology based-on Multi-Physical Approach and Electrical Simulations", IEEE Trans. Nucl. Sci., Vol. 60, No. 6, pp. 4421-4429, Dec. 2013.

[16]Hubert, G., D. Truyen, L. Artola, M. Briet, C. Heng, Y. Lakys, E. Leduc, "SET and SEU Analyses Based on Experiments and Multi-Physics Modeling Applied to the ATMEL CMOS Library in 180 and 90-nm Technological Nodes", IEEE Trans. Nucl. Sci., Vol. 61, No. 6, pp. 3178-3186, Dec. 2014.

[17]Raine, M., G. Hubert, P. Paillet, M. Gaillardin, A. Bournel, "Implementing Realistic Heavy Ion Tracks in a SEE Prediction Tool: Comparison Between Different Approaches", Nuclear Science, IEEE Trans. Nucl. Sci., Vol. 58, No. 4, pp. 950 – 957, August 2012.

[18]Hubert, G., P. Li Cavoli, C. Federico, L. Artola and J. Busto, "Impact of the Radial Ionization Profile of proton on SEU Sensitivity of nanoscale SRAMs", IEEE Trans. Nucl. Sci., Vol. 62, No. 6, pp. 840-847, Dec. 2015

[19]DeForest, S. E., Spacecraft charging at synchronous orbit, J. Geophys. Res., 77(4), 651–659, 1972

[20]Garrett, H. B., The charging of spacecraft surfaces, Rev. Geophys., 19(4), 577–616, 1981. doi:10.1029/RG019i004p0057.

[21]Gussenhoven, M.S. and E. G. Mullen, Geosynchronous environment for severe spacecraft charging, J. Spacecraft and Rockets 20, N°1, p. 26, 1983.

[22]Sarrailh, P., J.-C. Matéo-Vélez, J.-F.Roussel, B. Dirassen B., J. Forest, B. Thiébault, D. Rodgers, A. Hilgers, "Comparison of numerical and experimental investigations on the ESD onset in the Inverted Potential Gradient situation in GEO", *IEEE Trans. Plasma Sci.*, Vol 40, N°2, 2012.

[23]Sarrailh, P., S. L. G. Hess, J.-C. Mateo-Velez, B. Jeanty-Ruard, A. Trouche, J. Forest, "3D Modelling of Plasma Plume Interaction with Spacecraft in the Context of All-electric Platforms", in Proc. 35th International Electric Propulsion Conference, Atlanta, Georgia, USA, October 8 -12, 2017.